The Constant Power Spectral Density Model for Capacity Optimization of Submarine Links

Alberto Bononi, *Senior Member, IEEE*, Juliana Tiburcio de Araujo, Chiara Lasagni, *Member, IEEE*, Paolo Serena, and Jean-Christophe Antona, *Member, IEEE*

(Invited Paper)

***Abstract*—We review the fundamentals of the recently proposed Constant Power Spectral Density (CPSD) model for very long-haul space-division multiplexed submarine links, and highlight its use for Erbium-doped fiber amplifier (EDFA) optimization to maximize the achievable information rate (AIR) of the link. The CPSD line is an abstraction of modern submarine lines, where all EDFAs have identical physical parameters, among which the doped-fiber length ℓ, and the same pump and Erbium inversion, with identical gain-shaping filters that reproduce the line input power spectral density at the output of each span. The key idea in the CPSD line analysis is to use the hidden state-variable of the EDFA, namely the Erbium population inversion x, as a free variable. When x is known, so is the EDFA gain and its noise figure frequency profiles. Thus in the CPSD line we derive a simple expression of the received signal to noise ratio and thus of the AIR in the assumption of Gaussian noises. Among the set of input wavelength-division multiplexed signals that achieve inversion x at EDFA length ℓ we can find analytically the one maximizing AIR(x,ℓ). We finally look numerically for the best (x,ℓ) values that maximize AIR, i.e., we optimize the line EDFAs for maximum AIR. The major novelty of this invited paper is the extension of the analysis to include nonlinear effects into the AIR optimization.**

***Index Terms*—Optical communications, optical amplifiers, submarine transmission, signal droop.**

I. Introduction

THE capacity optimization of power-constrained submarine links has been the focus of much recent research [1], [2], [3], [4], [5], [6], [7], [8], [9], [10], [11], [12], [13], [14], [15], [16], [17], [18], [19]. Since the end-to-end electrical supply of submarine links is limited, so is the power that can be delivered to each optical amplifier; this in turn sets an upper bound to the capacity of the link [1]. According to the Shannon capacity formula, it is more power-efficient to increase the number of signal dimensions (bandwidth, space, polarization and quadrature) at low power, rather than increasing signal power into just a few dimensions. The modern approach so far to increase signal dimensions (given that the two polarizations and two quadratures are routinely used) is to either expand the used bandwidth by extending the wavelength division multiplexing (WDM) transmission beyond the traditional C band covered by the Erbium-doped fiber amplifiers (EDFA) [5], or to use transmission in the C band over many parallel spatial modes: in a first industrial deployment these will consist of several single-mode fiber pairs [13] with sharing of optical pumps among fibers [6], [17], while in the future multicore fibers and EDFAs will likely replace their single-mode counterparts to reduce cost [4], [14], [19].

This paper concentrates on the analysis of space-division multiplexed (SDM) submarine links with non-interacting spatial modes and having on each mode single-stage co-pumped EDFAs, all having the same physical characteristics, such as doping concentration, emission and absorption coefficient, doped-fiber length and optical pump power. All EDFAs are followed by a fixed gain shaping filter (GSF) which flattens the amplifier gain down to the span loss over the WDM bandwidth. When all the amplifiers have the same pump, they are said to be operated in constant output power (COP) mode [20]. However, we here assume that the GSF is tailored such that not only it ensures a COP mode, i.e., the same average power out of every amplifier, but it also reproduces at the output of each span exactly the same WDM power spectral density (PSD) as that at the transmitter (TX). This is the constant PSD (CPSD) link, an abstraction of the way many of today's submarine links are designed. Such links are in fact ideally CPSD links with a WDM flat PSD, i.e., all WDM channels are launched with the same power. Because of the fixed GSF construction inaccuracies at each EDFA, additional gain and tilt equalizers need to be inserted regularly down the line, with the aim of recovering the WDM flat PSD.

Perin et al. [11] proved the importance of accurately modeling the EDFA physics when optimizing capacity at a fixed EDFA pump power P_p. While their approach is fully numerical and based on the Giles-Desurvire rate and propagation equations [20], in [21] we introduced a novel semi-analytical

Manuscript received 20 June 2022; revised 19 August 2022; accepted 10 September 2022. Date of publication 14 September 2022; date of current version 2 February 2023. This work was supported by Ministero dell' Istruzione, dell' Universita e della Ricerca (FIRST, PRIN 2017) . *(Corresponding author: Alberto Bononi.)*

Alberto Bononi, Chiara Lasagni, and Paolo Serena are with the Dipartimento di Ingegneria e Architettura, Università di Parma, 43124 Parma, Italy, and also with the National Laboratory of Advanced Optical Fibers for Photonics (FIBERS), CNIT, L'Aquila, Italy (e-mail: alberto.bononi@unipr.it; chiara.lasagni@unipr.it; paolo.serena@unipr.it).

Juliana Tiburcio de Araujo and Jean-Christophe Antona are with the Alcatel Submarine Networks, Ctr. de Villarceaux, 91625 Nozay, France (e-mail: juliana.tiburcio_de_araujo@asn.com; jean-christophe.antona@asn.com).

Color versions of one or more figures in this article are available at https://doi.org/10.1109/JLT.2022.3206535.

Digital Object Identifier 10.1109/JLT.2022.3206535

approach where 1) we use the extended Saleh analytical model for the EDFA physics, which is a closed-form approximate solution to the Giles-Desurvire equations, and 2) we break the capacity optimization into a first step where we fix the EDFA inversion x and length ℓ and *analytically* find the capacity $C(x,\ell)$ using the Saleh model, and a second step in which we *numerically* optimize (x,ℓ), i.e. optimize the EDFAs, to maximize capacity. This 2-step procedure allows us to "look inside" the complex dependence of capacity on the WDM input PSD, and gain useful design insights [21]. The prominent role of the EDFA state-variable x in EDFA analysis dates back to [22], [23].

This paper reports on advancements of the analytical CPSD model first introduced in [21]. It provides more details on its use in the optimization of SDM submarine links when considering only the amplified spontaneous emission (ASE) noise. The major novelty of this paper is the extension of the analysis of CPSD links when also including the Kerr nonlinear interference (NLI) through the Gaussian noise (GN) model [24], [25]. While in [21] we applied the above 2-step procedure to the analysis of both the constant-signal link tackled in [11] and of the CPSD link, in this paper we concentrate only on the CPSD link because of its close resemblance to the operation of practical submarine links, and its greater analytical tractability.

The paper is organized as follows. Section II defines the CPSD model, while Sections III, IV define the NLI and EDFA models, respectively. Section V derives the TX power optimization to maximize the achievable information rate (AIR) at fixed EDFA inversion x, defines the x-feasible optimization search space, and illustrates the numerical problems connected with the inclusion of NLI. Section VI introduces the x-feasible allocation for two commonly used power allocations. Section VII presents the main numerical results. Finally Section VIII summarizes our findings. Appendix A contains the detailed derivation of the pump-constrained AIR maximization in presence of both ASE and NLI, while Appendix B presents new analytical results of the classical unconstrained AIR maximization with ideal amplifiers, which are used in the main text to interpret the pump-constrained optimized TX powers. This paper is an extended version of the short conference paper [26].

II. The CPSD Model

We focus on the transmission of a WDM signal on a generic spatial mode of an SDM submarine link, which we may think of as a single-mode fiber link. Fig. 1(a) highlights a generic span within the considered single-mode fiber CPSD link. Each span has a wavelength dependent span loss $A_j > 1$, an EDFA gain G_j, a GSF gain h_j and a shaped amplifier gain $\mathcal{G}_j = G_j h_j$ at all WDM channels $j = 1, .., N_c$. Since all EDFAs have the same pump and receive the same WDM PSD, they all have the same inversion x. The PSD conservation property of the CPSD link assures that the power $P_j = h f_j Q_j$ (with h Planck's constant, f_j the frequency and Q_j the flux (in photons per second [ph/s]) of channel j) is the same at the input and at the output of each span. Note that, for every channel j, P_j is the compound power

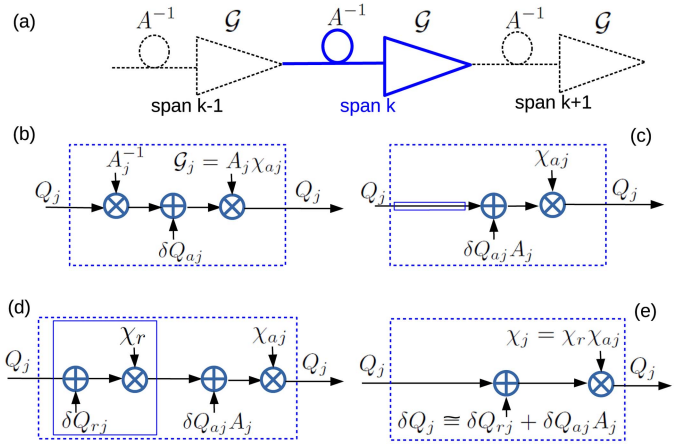

Fig. 1. (a) Generic span of a single-mode fiber CPSD submarine link with span loss $A_j > 1$ and shaped amplifier gain $\mathcal{G}_j$ at frequency f_j and identical at all amplifiers. (b) Span flux-diagram at WDM channel j, showing the input/output flux Q_j conservation at each CPSD span, with span attenuation A_j^{-1}, added ASE flux δQ_{aj}, and shaped amplifier gain $\mathcal{G}_j = A_j\chi_j$, with χ the gain droop. (c) Diagram equivalent to (b), with attenuation factored out, and ideal fiber (thick line). (d) WDM power-conserving perturbative noise δQ_{rj} generated during propagation is added as an input sub-block with power-renormalizing droop χ_r. (e) Final span-equivalent block diagram, where additive noise δQ_j is given in (2) and may be approximated for analytical optimizations as $\delta Q_j \cong \delta Q_{rj} + A_j\delta Q_{aj}$.

of the two polarizations of the transmitted spatial mode. In the following, to ease the EDFA treatment, we find it convenient to track the photon fluxes instead of the powers.

Fig. 1(b) shows the generic span flux flow diagram at channel j, with δQ_{aj} the input-equivalent ASE flux generated at the EDFA. To enforce the CPSD mode, the EDFAs need to have a gain $G_j(x) \geq A_j$ at every allocated WDM channel j. The GSF response h_j is chosen such that the amplifier shaped gain is $\mathcal{G}_j = A_j\chi_{aj}$ with $\chi_{aj} < 1$ the (wavelength-dependent) net span gain, also called the (gain) droop. Fig. 1(c) shows a block diagram equivalent to (b), where the span attenuation is "factored-out" and the fiber becomes an identity block, indicated by a thick line. Indeed several power-conserving perturbations of the signal, such as for instance NLI and/or crosstalk, may arise during fiber propagation. To model them, as shown in Fig. 1(d) we add at the span input a power-rearrangement sub-block, where the rearrangement perturbation δQ_{rj} is added to the signal Q_j and then multiplied by a *rearrangement droop* χ_r chosen such that total WDM power is conserved at the fiber end: $\sum_{j=1}^{N_c} h f_j Q_j = \left(\sum_{j=1}^{N_c} h f_j (Q_j + \delta Q_{rj})\right)\chi_r$, yielding

$$\chi_r = \left(1 + \frac{\sum_{j=1}^{N_c} f_j \delta Q_{rj}}{\sum_{j=1}^{N_c} f_j Q_j}\right)^{-1}. \tag{1}$$

The flux balance at the span diagram in Fig. 1(d) reads as: $[(Q_j + \delta Q_{rj})\chi_r + A_j\delta Q_{aj}]\chi_{aj} = Q_j$, which, after defining the total span droop $\chi_j = \chi_r\chi_{aj}$ and the total noise flux

$$\delta Q_j = \delta Q_{rj} + A_j\delta Q_{aj}\chi_r^{-1} \tag{2}$$

rewrites as $(Q_j + \delta Q_j)\chi_j = Q_j$ and yields both the total droop expression

$$\chi_j = \frac{1}{1 + \frac{\delta Q_j}{Q_j}} < 1 \tag{3}$$

and the equivalent span diagram in Fig. 1(e). Both droops χ_r and χ_j will normally be very close to 1 since the noises δQ_j injected at the span will normally be small perturbations of the main signal flux Q_j, so that the total noise flux (2) may be safely simplified to $\delta Q_j \cong \delta Q_{rj} + A_j \delta Q_{aj}$, as we will do in the subsequent analytical optimization.

Finally from $G_j h_j = \mathcal{G}_j = A_j \chi_j$ we get the x-dependent GSF response $h_j = A_j \chi_j / G_j \cong A_j / G_j$ which will be very close to the filter that perfectly flattens the gain down to the span attenuation [21, Fig. 5a].

A CPSD link of M spans is a concatenation of M block diagrams as in 1(e). Hence the received (RX) signal flux on channel j after M spans is $Q_j \chi_j^M$, and by the CPSD constraint the RX noise power is Q_j minus signal power, i.e., $Q_j(1 - \chi_j^M)$. Hence the RX SNR is:

$$\mathrm{SNR_j} = \frac{1}{\chi_j^{-M} - 1} \tag{4}$$

which is a channel-dependent version of the generalized droop formula [18], [27], [28], [29], [30], [31], [32], [33]. Assuming the noises δQ_j, $j = 1, .., N_c$ are independent Gaussian random variables, independent of the signal, the achievable information rate of this WDM parallel Gaussian vector channel in (bit/s) is

$$\mathrm{AIR}(\underline{Q}) = 2\Delta f \sum_{j=1}^{N_c} \log_2(1 + \Gamma \mathrm{SNR}_j) \tag{5}$$

with $0 \leq \Gamma \leq 1$ a penalty factor and Δf the per-channel bandwidth (Hz), and is a function of the transmitted flux vector $\underline{Q} = [Q_1, .., Q_{N_c}]$ (ph/s). This is the AIR of every 2-polarization spatial mode of our SDM submarine link.

III. NLI Model

For a comprehensive overview of the GN model and relevant references in the field the reader is referred to [25]. For our highly-dispersive submarine links, we may account only for the dominant self-phase and cross-phase modulation effects and get for the per-span NLI perturbation noise in (2) from the GN model [34]:

$$\frac{\delta Q_{rj}}{Q_j} = c_1 \left(\sum_n \gamma_{nj} Q_n^2 \right) \tag{6}$$

where: 1) $c_1 = \frac{16}{27}\gamma^2 L_{eff}^2$ (γ [W^{-1} km^{-1}] is the fiber nonlinear coefficient and L_{eff} the effective length); 2)

$$\gamma_{nj} = \frac{h^2 f_n^2}{\Delta f^2}(2 - \delta_{nj})\Psi_{nj} \tag{7}$$

with δ_{nj} the Kronecker delta (i.e., $\delta_{nj} = 1$ if $n = j$ and 0 else), and the equivalent per-span contribution for cross-channel interference ($n \neq j$) is [34], eq. (124)]:

$$\Psi_{nj} = \frac{A_+ - A_-}{4\pi |\beta_2| \alpha^{-1}} \tag{8}$$

where β_2 is the fiber dispersion coefficient, α is the bandwidth-averaged (power) fiber loss coefficient[1], and $A_\pm = \mathrm{asinh}(\pi^2 |\beta_2| \alpha^{-1}(f_n - f_j \pm \Delta f/2)\Delta f)$. It can be verified that $\Psi_{nj} = \Psi_{jn}$. Similarly, for self-channel interference ($n = j$) we have [34], eq. (125)]:

$$\Psi_{jj} = M^{\varepsilon} \frac{\mathrm{asinh}(\frac{\pi^2}{2} |\beta_2| \alpha^{-1} \Delta f^2)}{2\pi |\beta_2| \alpha^{-1}} \tag{9}$$

with ε the coherency slope [34, eq. (126)]. We explicitly report (6)–(9) since the above per-span NLI coefficients are tailored to our channel spacing Δf and obtained from the end-to-end NLI coefficients in [34] by dividing by the number of spans, a key requirement for the generalized droop model to properly work, as detailed in [31, Appendix B].

Finally, note that we are able to use the GN formulas verbatim since the shaped amplifiers gain is essentially flat at the span attenuation level over all WDM allocated channels. Since the span-input PSD is the same at all spans and includes accumulation of ASE and NLI up to the previous span, these formulas do also automatically include the (ASE+NLI)-signal nonlinear interactions [35], [36].

IV. EDFA Model

The EDFA physical model we use is the extended Saleh model (for a tutorial introduction see [21, Appendix]), where the EDFA gain is

$$G_j(x) = e^{\ell((\alpha_j + g_j^*)x - \alpha_j)} \tag{10}$$

where x is the Erbium population inversion, ℓ is the doped-fiber length, and g_j^*, α_j (m^{-1}) are the Erbium gain and absorption coefficients (in all calculations we use the values in [11, Fig. 7]). The ASE flux amplified inside the EDFA (forward and backward) is: $Q_{ASE}^{F+B} \cong 2 \sum_j 2 n_{sp,j}(x)(G_l(x) - 1)\Delta f$ (ph/s), where $n_{sp,j}(x) = g_j^* x / ((g_j^* + \alpha_j)x - \alpha_j)$ is the spontaneous emission factor at f_j, and the noise figure is $F_j = 2 n_{sp,j} \frac{G_j - 1}{G_j}$. The EDFA equivalent-input forward ASE flux at f_j over band Δf is

$$\delta Q_{aj} = F_j \Delta f. \tag{11}$$

If the EDFA input WDM fluxes are Q_j^{in}, $j = 1, .., N_c$, then the steady-state photon flux balance at the EDFA is given by the extended Saleh equation (ESE) [21, Appendix]:

$$\sum_{j=1}^{N_c} Q_j^{in}(G_j(x) - 1) = K(x, Q_p) \tag{12}$$

where the parameter

$$K(x, Q_p) \triangleq Q_p(1 - G_p(x)) - \frac{r_M}{\tau} x - Q_{ASE}^{F+B}(x) \tag{13}$$

[1] which equals 2α in [34], where the field fiber loss coefficient is used.

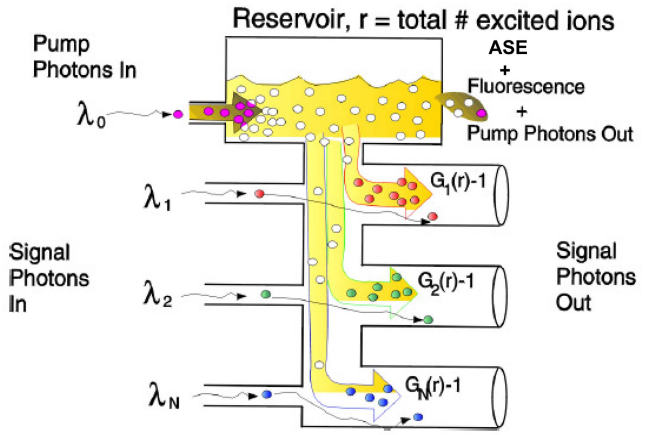

Fig. 2. Hydraulic equivalent of the Saleh EDFA model.

is the pump flux that gets converted to the EDFA output signal flux; here Q_p is the pump flux, $G_p < 1$ the pump gain as per (10), τ the fluorescence time, and r_M the total number of Erbium ions in the EDFA. The ESE therefore includes self-gain saturation by ASE.

Note that the number $N_c(x)$ of allowed WDM channels in CPSD mode does depend on the inversion x, since for all allowed channels j we need $G_j(x) > A_j$ (more details at [21, Appendix A]).

The Saleh model is totally equivalent to the hydraulic system shown in Fig. 2, consisting of a tank of maximum capacity r_M (the total number of Erbium ions in the doped fiber) which stores the Erbium ions that get excited by pump photons and whose number we call the reservoir r. The Erbium inversion $x \triangleq r/r_M$ is the fraction of excited ions and gives the normalized fill-in level of the tank. The tank has some leakage flux, due to unused pump photons ($Q_p G_p(x)$), fluorescence ($r_m x/\tau$) and forward+backward ASE ($Q_{ASE}^{F+B}(x)$) which all depend on the tank level x. The gain seen by the various input wavelengths such as the red, green and blue input photons, exponentially increases with the tank level x according to (10). At equilibrium the tank level x will depend on the balance of fluxes entering and exiting the tank, as expressed by the ESE (12), whose left-hand side represents the fluxes drawn by the input WDM signals out of the tank, while the right-hand side factor K in (13) represents the entering pump flux minus the leakage.

From Fig. 2, it is clear that at fixed pump Q_p, the tank level x increases as we decrease the input fluxes $\{Q_j\}$ since these will consume less ions in the reservoir. The maximum tank level x_M is reached at zero input signal. On the opposite side, we decrease x by increasing the input signal fluxes.

The Saleh model is called Extended to mean that tank leakage by the ASE flux (called ASE self-saturation) is analytically included, as first proposed by [37], while the original paper by Saleh et al. [38] did not include such a leakage.

We will see that this analytical model is the key to maximizing AIR in explicit algorithmic form.

V. AIR Maximization at Fixed x

Our semi-analytical strategy to get maximum capacity is the following. At a given pump Q_p and EDFA length ℓ, we partition the input signal space as the union of disjoint sets, one for each inversion value $x \in [0, x_M]$. At given x, we call such a set the x-feasible set $\mathcal{F}_x$, i.e., the set of TX flux vectors $\underline{Q}$ that satisfy Saleh equation (12) with $Q_j^{in} = Q_j/A_j$. Every such input WDM signal thus induces the desired inversion x in the CPSD line. Within each $\mathcal{F}_x$ we are able to analytically find the winner, i.e., the best signal that yields the maximum AIR. The reason is that the gain $G(x)$, the number of channels $N_c(x)$, as well as the useful flux $K(x)$ in (13) are all fixed. Once we have the winner at each x, we can numerically find the winner of the winners, the one that maximizes AIR over all subsets $\mathcal{F}_x$ for $x \in [0, x_M]$, i.e., over the entire signal space. Such a winner is the signal that achieves capacity at the given EDFA length ℓ. A final numerical maximization over ℓ yields the global maximum capacity and the optimal EDFA inversion and length.

We now analytically maximize AIR at a given x. Our problem is that of maximizing the AIR in (5), subject to the x-feasibility constraint (12). As shown in Appendix A, using the method of Lagrange multipliers we find the sought optimal (OPT) flux vector $\underline{Q}^{\text{OPT}}$ as the solution to the following nonlinear system of equations for all $k = 1, .., N_c$:

$$Q_k = \frac{A_k K(x, Q_p)}{G_k(x) - 1} \frac{g_k(\underline{Q})}{\sum_{l=1}^{N_c} g_l(\underline{Q})} \tag{14}$$

where g_k is defined in (24).

With only ASE, (14) becomes (18) in [21], and is solved by the simple fixed-point algorithm in [21], (19)]. The bad news is that at large-enough pump power (when NLI is significant) the fixed-point algorithm fails to converge, so that the solution of (14) requires a nonlinear solver.

Therefore with NLI we find it faster to directly numerically maximize $\text{AIR}(x, \underline{Q})$ over the feasible set, which we conveniently express as

$$\mathcal{F}_x \triangleq \left\{ \underline{Q} : Q_k = \frac{A_k K(x, Q_p)}{G_k(x) - 1} q_k, \forall \underline{q} : \left\{ \begin{array}{c} \sum_{k=1}^{N_c} q_k = 1 \\ 0 \le q_k \le 1 \end{array} \right\} \right. \tag{15}$$

where the probability mass function (PMF) $\underline{q}$ is called the *generating* PMF of feasible vector $\underline{Q}$. This means that each x-feasible $\underline{Q}$ is a convex combination of the edge vectors $\underline{Q}_k = \frac{A_k K(x,Q_p)}{G_k(x)-1} \underline{e}_k$, with $\underline{e}_k$ the vector of all zeros, except a 1 at the k-th position. The edge vector $\underline{Q}_k$ thus has edge power $\frac{A_k K(x,Q_p)}{G_k(x)-1}$ all concentrated at channel k. The probability q_k gives us the fraction of edge-k power actually used by a given feasible flux vector $\underline{Q}$. A sketch of the feasible set in dimension $N_c = 3$ is reported in Fig. 3. This formulation allows seeing $\text{AIR}(\underline{q})$ as a function of the generating PMF $\underline{q}$ and the search with a numerical maximizer is thus restricted to the probability simplex (i.e. the set of all PMFs) of dimension N_c. Note that (14) just states that the optimal generating PMF has entries $q_k = g_k / \sum_{l=1}^{N_c} g_l$.

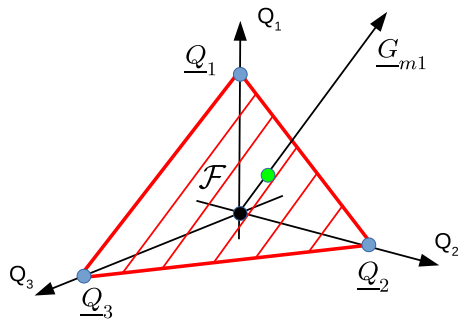

Fig. 3. The x-feasible set $\mathcal{F}_x$ is the hatched portion of plane delimited by edge vectors $\underline{Q}_1 = [A_1K/(G_1-1), 0, 0]$, $\underline{Q}_2 = [0, A_2K/(G_2-1), 0]$, $\underline{Q}_3 = [0, 0, A_3K/(G_3-1)]$ and orthogonal to vector $\underline{G}_{m1} = [(G_1-1)/A_1, (G_2-1)/A_2, (G_3-1)/A_3]$, for flux vectors of dimension $N_c = 3$.

To get a feeling as to why (14) can be solved by a simple iterative algorithm in absence of NLI while NLI complicates matters, it is instructive to visualize the constrained AIR($\underline{q}$) surface at given (x, Q_p) in the simplest case of only 3 WDM channels. In this case $\underline{q} \in \mathbb{R}^3$ and thus we provide the 3D surface AIR(q_1, q_2), with $q_3 = 1 - q_1 - q_2$. Fig. 4(a) shows the used WDM allocation of 3 channels all at an EDFA gain close to the span attenuation $A = 9.5$ dB and at inversion $x = 0.63$ and EDFA length $\ell = 6.27$ m. The pump was 25 mW and the three TX channel powers at the optimum working point without NLI (Cfr. circle in Fig. 4(b)) are reported in the figure. The rest of Fig. 4 shows the AIR(q_1, q_2) in (5) after $M = 100$ spans both without NLI (b) and with NLI (c), and the global maxima are shown with a circle on the surface. The propagation fiber was a pure silica core fiber (PSCF) with attenuation 0.162 dB/km, nonlinear index $n_2 = 2.5 \cdot 10^{-20}$ m $^2/W$, effective area 130 μm^2 (yielding a nonlinear coefficient $\gamma = 0.78$ W^{-1} km^{-1}) and dispersion 21 ps/nm/km. The fiber span length was 50.9 km. The WDM channels had a bandwidth of 50 GHz and a Gaussian modulation. In this highly-dispersive line we calculate the NLI variance by the GN model as Sec. III. In absence of NLI (Fig. 4(b)) we note a well-behaved concave surface, with a wide plateau around the maximum. This means that there are infinitely many sub-optimal power allocations whose AIR is practically optimal. This behavior is found also in realistic fully populated WDM systems [21]. When instead a significant NLI is present (Fig. 4(c)) we note the appearance of multiple local maxima and minima (the three maxima here correspond to allocating almost the entire power budget at a single channel), with a much more complicated AIR landscape.

Although with NLI in practice we do not solve (14) but directly maximize AIR(x, Q_p) over the feasible set with a nonlinear solver, still its derivation is conceptually important, since for instance it allows us to obtain approximate optimal power profiles for ideal amplifiers (i.e., in absence of the pump-power constraint) as explained in Appendix B, and thus better appreciate the optimal power profiles we get with real EDFAs, as we will see in the numerical section.

VI. Suboptimal Allocations

Although finding the OPT flux allocation $\underline{Q}$ in presence of NLI in not straightforward, there are other practical flux allocations that are routinely used in submarine links, whose TX fluxes at fixed x are easily expressed, and whose AIR is always very close to the optimal when working near the optimal inversion, as we will see. These are:

1) the constant SNR allocation (CSNR). Here in absence of NLI we want the RX SNR_k and thus droop χ_k to be the same at every channel k, i.e. per (3) we want $A_k \delta Q_{ak}/Q_k$ to be constant in k, i.e., $Q_k \propto A_k F_k$. Thus from (15) it must be $\frac{A_k K(x,Q_p)}{G_k(x)-1} q_k \propto A_k F_k$, hence $q_k = \frac{F_k(G_k-1)}{\sum_j F_j(G_j-1)}$, and so the CSNR fluxes are for $k = 1, .., N_c$

$$Q_k^{\text{CSNR}} = \frac{K(x, Q_p) A_k F_k(x)}{\sum_j F_j(x)(G_j(x)-1)}. \tag{16}$$

Note that finding the flux $\underline{Q}$ that equalizes the SNR with NLI is a tougher problem [39], admitting a solution only at sufficiently small pumps and thus mild NLI, that we do not report since it always provides an AIR inferior to the one obtained by the above CSNR allocation without NLI.

2) the constant input power (CIP) allocation, where all WDM channels have the same power P_c, hence : $Q_k \propto 1/f_k$. Thus it must be $\frac{A_k K(x,Q_p)}{G_k(x)-1} q_k \propto \frac{1}{f_k}$, and therefore $q_k = \frac{\frac{G_k-1}{A_k f_k}}{\sum_j \frac{G_j-1}{A_j f_j}}$, and so the CIP fluxes are for $k = 1, .., N_c$

$$Q_k^{\text{CIP}} = \frac{K(x, Q_p)/f_k}{\sum_j \frac{G_j(x)-1}{A_j f_j}}. \tag{17}$$

Note that (16) and (17) are the *unique* CSNR and CIP fluxes within the x-feasible set.

VII. Numerical Results

As in [11], [21], we analyze an $M = 287$ span submarine link with single-stage EDFAs and flat span attenuation $A = 9.5$ dB. Spans have length 50.9 km of PSCF fiber with data as in Fig. 4.

Fig. 5 shows the AIR versus inversion x at several pump powers $P_p = [30, 80, 180]$ mW and at EDFA length 6.27 m (which is quasi-optimal in a wide pump range around $P_p = 60$ mW [11]), with only ASE (dashed), and with ASE+NLI (solid), when the OPT allocation (14) is used.

Such AIR curves have a quick increase after x exceeds a cutoff inversion (here 0.57, when the EDFA profile starts exceeding the span loss A and the number of allocated WDM channels $N_c(x)$ starts increasing), reach a top-AIR value (indicated by a circle at the top of the curves) and then decrease with x. We note from the gap between dashed and solid curves that the presence of NLI induces an AIR decrease which starts to be visible at pumps $P_p \geq 80$ mW. While in absence of NLI the top AIR is achieved at an inversion that settles at large-enough pump (>30 mW) to a constant value $x \cong 0.63$ (which for the selected EDFA length corresponds to an EDFA gain profile such that the gain trough at 1538 nm equals the span attenuation, see [21, Fig. 7]), we note that with NLI there is a marked increase of the optimal inversion

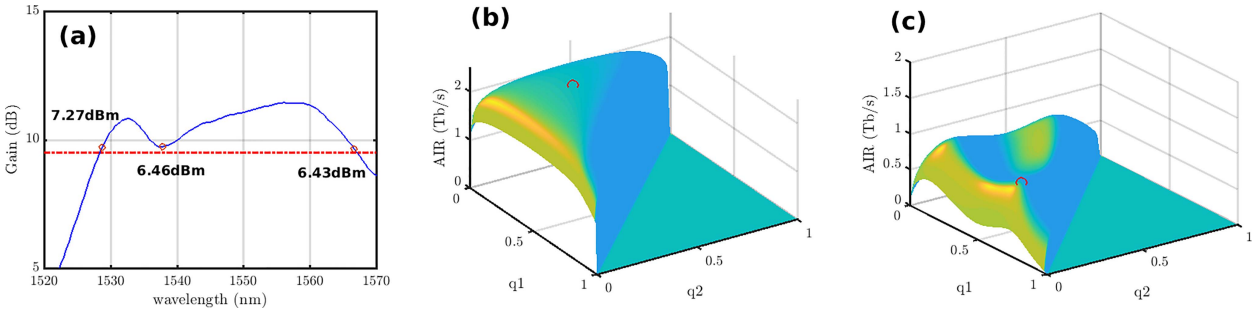

Fig. 4. (a) EDFA gain versus wavelength profile at inversion $x = 0.63$ and EDFA length 6.27 m. We mark the 3 WDM channels (circles) and report their optimal powers at pump power $P_p = 25$ mW and no NLI. Dashed horizontal line is span attenuation $A = 9.5$ dB. (b) AIR (5) versus generating PMF entries (q_1, q_2) after $M = 100$ spans at gap $\Gamma = 1$. (c) Same as (b) but with NLI, with channels having a Gaussian modulation and bandwidth $\Delta f = 50$ GHz, and PSCF spans of 50.9 km. Red circles at global maxima.

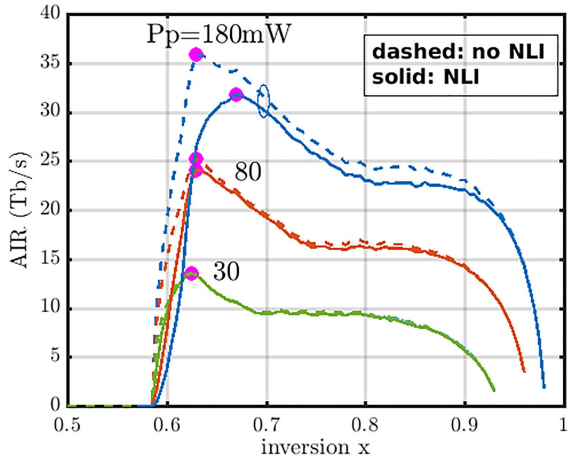

Fig. 5. AIR vs. inversion x for an 287×50.9 km PSCF link, span loss $A = 9.5$ dB, EDFA length 6.27 m with emission and absorption coefficients as in [11, Fig.7] and pump powers $P_p = [30, 80, 180]$ mW, both without NLI (dashed) and including NLI (solid). Optimal (OPT) WDM power allocation (14) . Channel bandwidth $\Delta f = 50$ GHz. Top AIR values marked by circles.

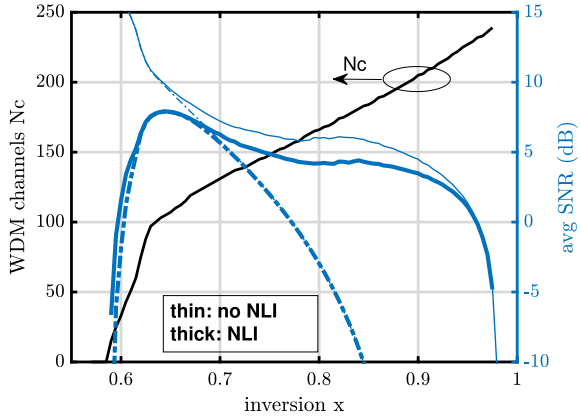

Fig. 6. (left axis) number $N_c(x)$ of used 50 GHz WDM channels, and (right axis) the SNR averaged in linear units over the N_c channels, after $M = 287$ PSCF spans with span loss $A = 9.5$ dB, at EDFA pump $P_p = 180$ mW and length $\ell = 6.27$ m. SNR is reported for the OPT (14) (solid) and CIP (17) (dash-dot) allocations. Thin lines: no NLI; thick lines: with NLI.

at the largest pump, because the TX OPT profile flattens more and more towards a limit value (as we will discuss shortly) and thus the more we increase the pump the more the extra pump causes an inversion increase at fixed signal power.

To understand the AIR vs. x behavior, keep in mind that increasing the inversion at fixed pump power implies decreasing the total WDM power. The above AIR behavior at increasing x comes from a bandwidth/SNR trade-off, illustrated in Fig. 6 for the case $P_p = 180$ mW. Fig. 6 plots against inversion x both (left vertical axis) the number $N_c(x)$ of allowed 50 GHz WDM channels, and (right vertical axis) the SNR averaged in linear units over the N_c channels. SNR is provided both for the OPT allocation (14) (solid) and the CIP allocation (17) (dash-dot). The CSNR allocation (16) always yields quite similar results to CIP and is not reported. We see that as x increases also the number of channels $N_c(x)$ allocated in the spectral region with EDFA gain above span loss increases. At the same time, as x increases the WDM power decreases, while the noise figure improves such that also the ASE noise decreases. In absence of NLI this causes a monotone decrease of SNR in the CIP case, while the OPT allocation better manages the signal power decrease at increasing x, so that on a limited inversion range near $x = 0.8$ the SNR slightly re-increases since there the ASE decrease is faster than the power decrease. When we also include NLI (thick lines) we see that the small-x high WDM power region has a very low SNR dominated by NLI, while as x increases and total power decreases, NLI is less and less important and the SNR merges with its (thin line) curves without NLI. The top average SNR is reached at inversion 0.645, which is different from the inversion 0.67 at which AIR is maximum at this 180 mW pump (see the circle at top AIR in Fig. 5). This simply means that average SNR is not fully indicative of AIR behavior, since also the bandwidth (i.e. number of WDM channels) substantially contributes to the AIR, as per (5).

Fig. 7 shows, for the case including NLI, the same OPT curves shown in Fig. 5, now plotted along with those of the CIP (dash-dot) and CSNR (dashed) allocations. For the largest 180 mW pump we also show in dotted line the AIR achieved by using the OPT allocation in absence of NLI (we call it OPT-noNLI, obtained by setting $c_1 = 0$ in (24), (28)) and we note that using the OPT-noNLI allocation yields an AIR not too far from the optimal one at all inversions. The important message we get from this figure is that the CIP allocation, in a neighborhood of

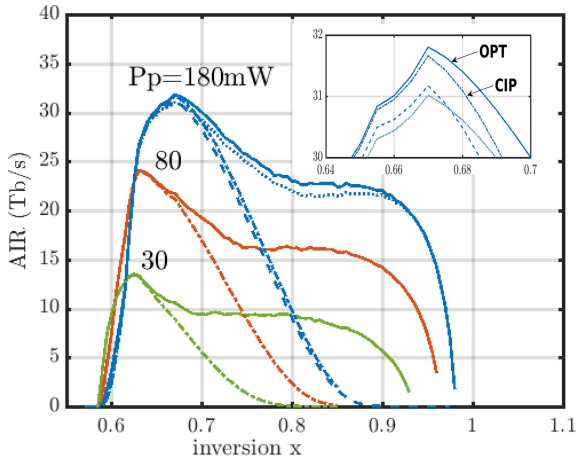

Fig. 7. With NLI, same AIR vs. inversion x as in Fig. 5 for OPT (solid), but now we also add the AIR of allocations CSNR (dashed) and CIP (dash-dotted). At pump $P_p = 180$ mW we also show the OPT-noNLI allocation (dotted). Inset shows zoom of top AIR at pump 180 mW.

the optimal inversion, achieves essentially the same top AIR as the OPT allocation, and is also slightly preferable to both the CSNR and the OPT-noNLI allocations, as we appreciate by the zoom shown in the inset of Fig. 7. We also notice the dramatic AIR decrease of the CIP and CSNR allocations as we move beyond and away from the optimal inversion.

As an example, at inversion $x = 0.85$ we see from Fig. 7 that the CIP/CSNR AIR drops to about 1/9 of the OPT AIR. Fig. 8 reports at such an inversion (top) the EDFA gain profile, and (bottom) the TX WDM power allocated by the three policies OPT, CIP, CSNR. Overall the total TX WDM power is small for all cases, which is necessary to achieve such a high inversion. With little total signal power *at the EDFA output*, and the gain flattening filter chopping off all the gain above attenuation (see the huge gap between EDFA gain and attenuation in Fig. 8(top)) the OPT wisely allocates power mostly on channels close to 1510 and 1580 nm where the EDFA gain equals the span attenuation, and thus the GSF wastes little signal photons. CIP and CSNR instead insist on allocating power even in regions where the GSF will mostly suppress it. This clearly explains the dramatic drop in AIR for CIP and CSNR. However we verified that if we admit a CIP allocation only in the spectral regions used by the OPT allocation, then CIP recovers most of its lost AIR. In other terms, provided the "correct" spectral range is used, then using a flat input profile is quasi optimal, as is also known from the wireless literature [40].

Let's now go back to the circles indicating the top AIR in Fig. 5. Fig. 9 shows the corresponding TX WDM power versus wavelength profile for the OPT allocation. We first confirm that, without NLI, the OPT (i.e. capacity-achieving) power profile (dashed lines) has an inverse-gain shape, as analytically proved in [21], [41], and would (incorrectly) predict larger and larger TX powers as the pump increases. The reason of the inverse-gain shape is seen from (14), since for all inversions in a neighborhood of the optimal inversion the generating PMF $g_k / \sum_j g_j$ is practically uniform over the N_c channels, hence

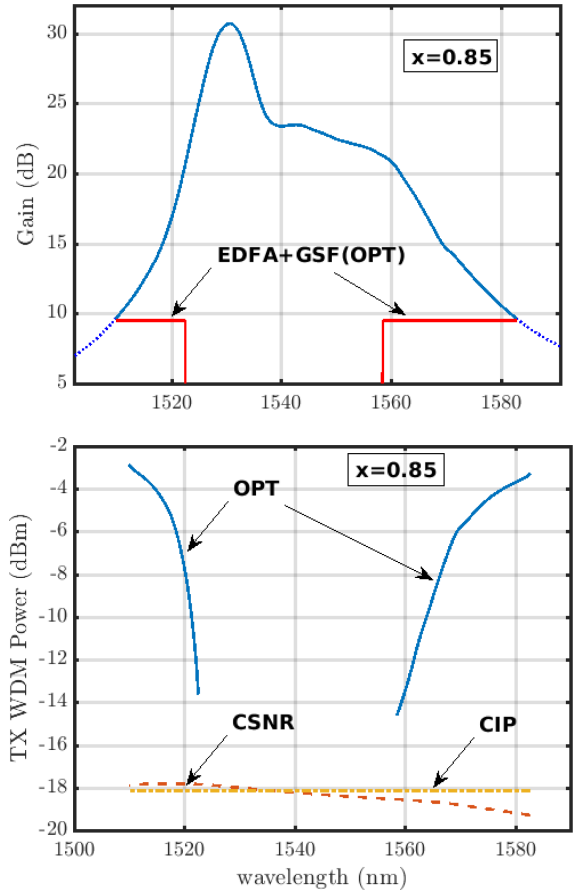

Fig. 8. (Top) EDFA gain vs. wavelength at $x = 0.85$, $\ell = 6.27$ m, along with equalized gain for OPT allocation. (Bottom) TX WDM power for OPT, CIP and CSNR allocations at pump $P_p = 180$ mW. NLI included.

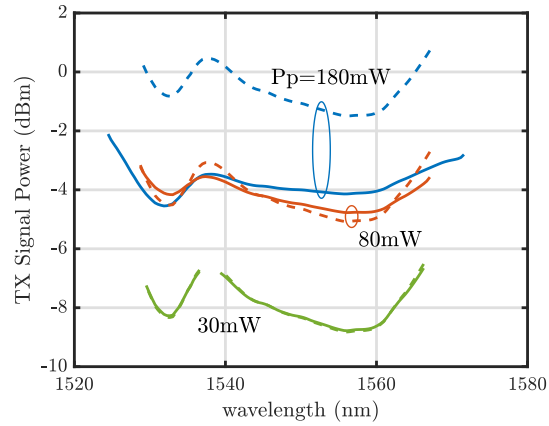

Fig. 9. For the same 287-span link as in Fig. 5, we show the TX WDM power versus wavelength for the OPT allocation (14) at the 4 top AIR values indicated by circles in Fig. 5. Dashed: ASE only; Solid: ASE+NLI. EDFA length $\ell = 6.27$ m.

$Q_k^{\mathrm{OPT}} \cong \frac{1}{N_c(x)} \frac{A_k K(x,Q_p)}{G_k(x)-1}$ is proportional to $1/(G_k - 1)$ for a flat attenuation A. Also note that the optimal allocation puts the smallest flux at the largest gain, and the largest flux at the smallest gain equal to A, thereby somewhat equalizing over wavelengths the signal flux chopped off by the GSF.

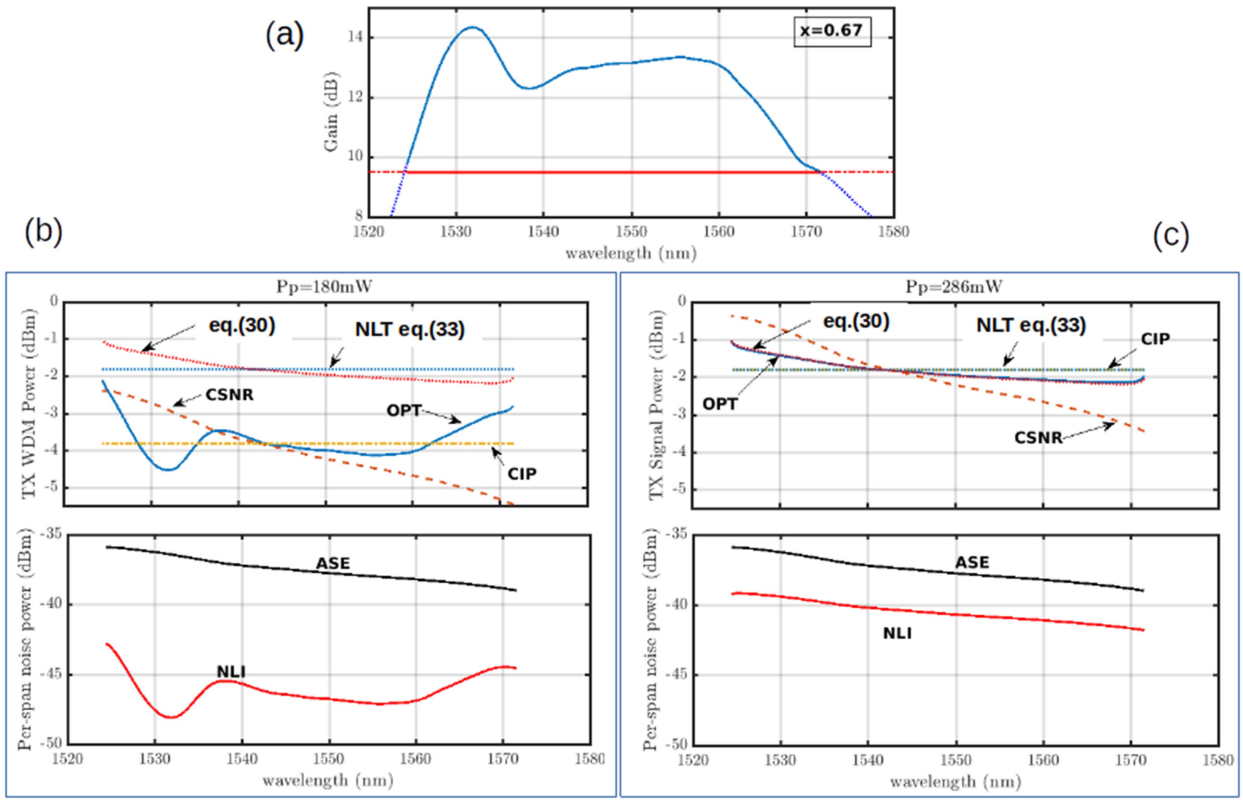

Fig. 10. (a) EDFA gain vs. wavelength at $x = 0.67$, $\ell = 6.27$ m, along with equalized gain at span loss $A = 9.5$ dB (horizontal line). Number of channels $N_c(x) = 119$. (b) At $P_p = 180$ mW and with NLI, we show (top) the TX WDM power vs wavelength for allocations CSNR, CIP and OPT. Also shown are the GN-predicted NLT (33) and optimal unconstrained power (30); (bottom) we show the per-span generated ASE and the OPT-generated NLI vs. wavelength. (c) Same as box (b), but now pump has been increased to $P_p = 286$ mW.

Instead, the OPT power profile with NLI is flatter and tends to stabilize around a common average power per channel as the pump increases. What is surprising is the fact that the optimal TX profile still has the shape of the inverse gain as in absence of NLI, although it is much flatter.

To understand more on this issue, Fig. 10(a) shows the EDFA gain profile at the top of the AIR vs. x curve in Fig. 5 for the OPT allocation with NLI and at $P_p = 180$ mW, i.e., at inversion $x = 0.67$. Box (b) shows (top) the TX WDM power vs wavelength for allocations OPT, CIP and CSNR, and (bottom) the per-span generated ASE and OPT-generated NLI powers versus wavelength. We see from Fig. 10(a) that, contrary to the linear case, with NLI-optimized x the EDFA gain trough at 1538 nm is now 3 dB above the span loss A. The OPT TX profile in Fig. 10(b, top) is the same as the solid 180 mW curve in Fig. 9. Here OPT allocates channels across the whole available $N_c(x) = 119$ channels with EDFA gain above A, like the CIP and CSNR TX powers (also reported in the figure), and indeed their AIR is about the same as that of OPT. Fig. 10(b, bottom) shows the per-span generated ASE and OPT-generated NLI powers versus wavelength, and we note that the ASE to NLI ratio is on average 9 dB, well above the 3 dB predicted by the GN model at powers optimizing NLI+ASE with ideal amplifiers, as discussed in Appendix B. Therefore the optimal operating point at $x = 0.67$ is still clearly in the linear regime, below the optimal power with NLI (the so-called nonlinear threshold (NLT) [42]). The NLT is derived from the GN model in Appendix B and reported in Fig. 10(b, top) as (33), along with a novel analytical expression of the optimal pump-unconstrained TX allocation (30), also derived in Appendix B.

By keeping the same inversion and further increasing the pump to $P_p = 286$ mW, we reach a very peculiar situation at which the optimal CIP power (17) coincides with the NLT. The situation is depicted in Fig. 10(c). Now the OPT allocated power does coincide with the pump-unconstrained optimal power profile (30) across all the allowed $N_c(x)$ WDM channels, and the ASE/NLI ratio is very close to 3 dB. Further increasing the pump leads to an OPT TX power profile above the unconstrained profile. However, at $P_p = 286$ mW the inversion maximizing the AIR with the OPT allocation is now $x = 0.695$, at which we still operate in the linear regime.

To better visualize such operation in the linear regime at top inversion, we can convert the AIR versus x curves in Fig. 7, which are unfamiliar to most readers, into the AIR versus total TX WDM power P_{tot} at each x. Fig. 11 shows such AIR curves with NLI at pump 180 mW for the CIP and OPT allocations. We first note that, when AIR is plotted versus P_{tot}, it may be multiple-valued, as seen for instance at the strange wiggle at TX power around 14 dBm, since the same TX power may produce different inversions which may yield slightly different AIR values. Since

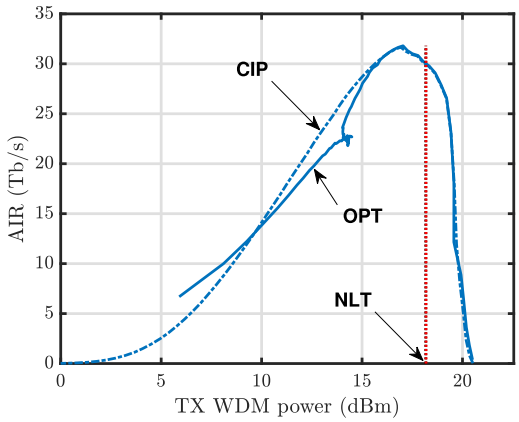

Fig. 11. Same AIR curves with NLI as in Fig. 7 for OPT (solid) and CIP (dash-dot) allocations and at EDFA pump 180 mW, now plotted versus total x-feasible WDM power $P_{\text{tot}}(x) = \sum_{j=1}^{N_c(x)} P_j(x)$. Vertical dotted lineshows the GN-predicted pump-unconstrained nonlinear threshold $N_c P^*$, (33).

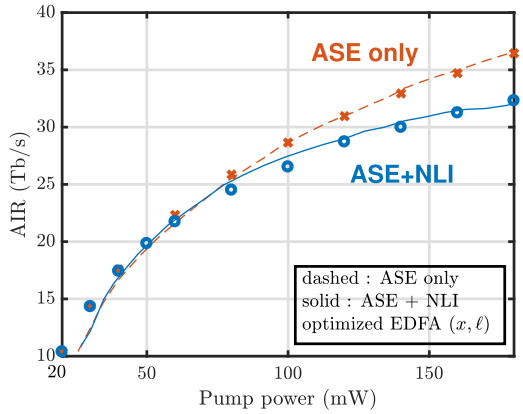

Fig. 12. AIR vs. pump power for the studied 287 × 50.9 km PSCF link with 50 Gbd Gaussian-modulated channels with spacing 50 GHz. At each pump we optimize the EDFA length ℓ and inversion x, and the GSF for CPSD operation depends on (x, ℓ). Symbols: our semi-analytical computation. Lines: curves taken from [11, Fig. 4a].

the OPT allocation maximizes AIR at fixed inversion, and not at fixed total TX power[2], its AIR need not be always larger than the CIP AIR, and indeed it is much larger only at very small input powers, when the scarce signal power needs to be wisely allocated. Next we note that both the OPT and CIP curves reach their top AIR almost at the same value of P_{tot} (to within 0.1 dB), and such a value is smaller by about 1.2 dB than the NLT $N_c(x)P^*$ predicted by the GN model, indicated by a vertical dotted line, where P^* is given by (33) in Appendix B, and we used for simplicity the number of channels $N_c(x)$ at the inversion x corresponding to top AIR (that's why we see 1.2 dB instead of the 2 dB of gap seen in Fig. 10(b, top)). Fig. 11 thus further confirms the fact that at top AIR we are below the NLT by 1-2 dB.

Finally, Fig. 12 reports with symbols the top AIR values at optimal x versus pump power for our CPSD link with optimized EDFA length ℓ at each pump. With only ASE, as pump increases the inversion is clamped to 0.63 and the AIR increase is due to an increased TX power. With ASE+NLI, as pump increases the inversion keeps increasing, so both noise figure and number of WDM channels improve, while the average TX power levels off. Hence the AIR increase with pump is due to an improvement of noise figure and supported bandwidth. Fig. 12 also reports in solid and dashed lines the top AIR values for the "constant-signal"[3] link tackled in [11, Fig. 4a], and known to be quite close to our CPSD link except at the very smallest pumps [21]. The good match of our theory with the calculations in [11] corroborates both their results and our CPSD model.

[2]Finding the allocation policy maximizing AIR at fixed P_{tot} is a much harder problem, likely not amenable to an exact analytical solution. However, both our AIR maximization at fixed x followed by maximization over x, and the alternative AIR maximization at fixed P_{tot} followed by maximization over P_{tot} must produce the same value of top AIR over the whole input signal space, i.e., capacity, which indeed is our final objective.

[3]In "constant-signal" links the GSFs chop the gain exactly down to A at all WDM channels, so that the signal power is conserved at each span, but ASE and NLI do accumulate and increase down the line, thus slightly decreasing the EDFAs inversion down the line.

VIII. Summary and Conclusions

Many modern submarine links have a frequency-flat (or constant) input WDM power (which we called CIP) and such a flat power spectral density is enforced along the link both by fixed GSFs at all EDFAs that try to flatten the EDFA gain down to the span loss at all WDM channels, and by adjustable gain equalizers regularly spaced along the link that correct for the non-ideality of the GSFs. So the link operation tends to reproduce the TX power spectral density at each span input. Our CPSD mathematical abstraction includes this link operation, and generalizes it to any input WDM power profile, including the OPT one that maximizes the AIR. When links have hundreds of spans and thus the RX SNR falls (for some channels) below 6-7 dB, a correct SNR evaluation is possible only by using the Generalized Droop Model (GDM) [31], [33]. The CPSD model does naturally extend the GDM to include the frequency-dependency of the SNR due to the non-flatness of the EDFA gain and noise figure frequency profiles. The attractive feature of the CPSD model is its analytical tractability, which we reviewed and illustrated with examples when including both ASE and NLI. We explored the shape of the optimal TX WDM power allocation in this pump power constrained scenario in comparison with the optimal allocation with ideally flat amplifiers and found examples where the two do coincide. Clearly other noise sources such as crosstalk can be seamlessly added to the model. Our semi-analytical AIR calculation allows a fast run time. For instance, on a Dell Inspiron 5000 laptop getting at a fixed length an AIR vs pump power curve like the one in symbols in Fig. 12 takes our Matlab™ code about 7 seconds for the ASE-only case, and about 5 minutes for the ASE+NLI case which uses the general-purpose nonlinear solver *fmincon*.A shortcoming of the CPSD model is its inability to capture polarization-dependent effects, since it only tracks the compound power of the two polarization states of each spatial mode. Also, spectral-hole burning (SHB) [44], [45] may change our conclusions on the OPT TX power profile, and it would be interesting to see if the CPSD model can be extended to SHB. Luckily, however, the CIP allocation performs almost as well

as the OPT allocation at the correct inversion, and is way less affected by SHB [46], [47]. Therefore the top AIR results for the CIP allocation we found here (by confirming the findings in [11]) are realistic, in agreement with recent experimental results [18].

APPENDIX A
PUMP-CONSTRAINED AIR MAXIMIZATION

Our problem is that of maximizing

$$\text{AIR}(x,\underline{Q}) = \frac{2\Delta f}{\ln(2)}\sum_{j=1}^{N_c}\ln(1+\Gamma(\chi_j(x,\underline{Q})^{-M}-1)^{-1}) \quad (18)$$

subject to the x-feasibility constraint (12). For this we form the Lagrangian:

$$L(\underline{Q}) = \text{AIR}(x,\underline{Q}) - \lambda\sum_{j=1}^{N_c(x)}\frac{Q_j}{A_j}(G_j(x)-1) \quad (19)$$

where λ is the Lagrange multiplier, and we use the following droop expression obtained from the simplified diagram in Fig. 1(e) and (3), (2), (6), (11):

$$\chi_j(x,\underline{Q}) = \left(1+c_1\left(\sum_n \gamma_{nj}Q_n^2\right)+\frac{A_jF_j(x)\Delta f}{Q_j}\right)^{-1}. \quad (20)$$

The goal is to set $dL/d\underline{Q} = \underline{0}$ and find the optimal WDM flux vector $\underline{Q}$. To this aim we compute $\frac{\partial \text{AIR}}{\partial Q_k} = \sum_{j=1}^{N_c}\frac{\partial \text{AIR}}{\partial \chi_j}\cdot\frac{\partial \chi_j}{\partial Q_k}$, with $\frac{\partial \text{AIR}}{\partial \chi_j} = \theta\frac{f(\chi_j)}{\chi_j^2}$, where $\theta \triangleq \frac{2\Delta f\Gamma M}{\ln(2)}$ and we defined

$$f(\chi) \triangleq \frac{\chi^{M+1}}{(1-\chi^M)(1-\chi^M(1-\Gamma))}, \quad (21)$$

and

$$\frac{\partial\chi_j}{\partial Q_k} = \chi_j^2\left[\frac{A_jF_j\Delta f}{Q_j^2}\delta_{jk} - 2c_1\gamma_{kj}Q_k\right]. \quad (22)$$

Thus we find

$$\frac{\partial \text{AIR}}{\partial Q_k} = \frac{\theta}{Q_k}g_k \quad (23)$$

with

$$g_k \triangleq f(\chi_k)\frac{A_kF_k\Delta f}{Q_k} - 2c_1Q_k^2\sum_{j=1}^{N_c}f(\chi_j)\gamma_{kj}. \quad (24)$$

Therefore setting $dL/dQ_k = 0$ for each channel k yields

$$Q_k\frac{G_k-1}{A_k} = \frac{\theta}{\lambda}g_k. \quad (25)$$

To eliminate the unknown Lagrange multiplier λ, sum both sides of (25) over all channels so as to get the left-hand side of Saleh (12) and thus $\frac{\theta}{\lambda} = K(x,Q_p)/\sum_{l=1}^{N_c}g_l$. Plugging back into (25) finally yields the sought optimal (OPT) flux $\underline{Q}$ allocation as the solution to the following nonlinear system of equations for all $k = 1,..,N_c$:

$$Q_k = \frac{A_kK(x,Q_p)}{G_k(x)-1}\frac{g_k(\underline{Q})}{\sum_{l=1}^{N_c}g_l(\underline{Q})} \quad (26)$$

which is (14) in the main text. We can get an alternative expression for g_k in (24) by manipulating (20) as:

$$\frac{A_kF_k\Delta f}{Q_k} = \frac{1-\chi_k}{\chi_k} - c_1\left(\sum_n\gamma_{n,k}Q_n^2\right) \quad (27)$$

and substituting into (24) to get:

$$g_k = g(\chi_k) - c_1\left[\sum_n Q_n^2f(\chi_k)\gamma_{nk} + 2\sum_j Q_k^2f(\chi_j)\gamma_{kj}\right] \quad (28)$$

with $g(\chi_k) \triangleq f(\chi_k)\frac{1-\chi_k}{\chi_k}$. Such an expression in absence of NLI ($c_1 = 0$) becomes (18) of [21].

APPENDIX B
UNCONSTRAINED AIR MAXIMIZATION

In this appendix we explore the optimal WDM power profile in presence of ASE and NLI for a link with amplifiers having gain equal to the span loss at all WDM channels, but *not subject to any pump constraints*, i.e., the ideal amplifiers considered in the GN model. The AIR-optimizing (OPT) WDM TX power allocation is found as in Appendix A by setting $\frac{\partial \text{AIR}}{\partial Q_k} = 0$ at all channels $k = 1,..,N_c$. From (24) and under the approximation that $f(\chi_k)$ is roughly the same at all channels, we thus get the equation: $2P_k^3c_1\sum_j\gamma'_{kj} = P_{A1,k}$, with $\gamma'_{kj} = \gamma_{kj}/(hf_k)^2$ and $P_{A1,k} \triangleq hf_kA_kF_k\Delta f$ the span-input equivalent ASE power at channel k generated in one span. We may thus define a single-span channel-dependent NLI coefficient

$$\alpha_{\text{NL1},k} \triangleq c_1\sum_{j=1}^{N_c}\gamma'_{kj} = \frac{16}{27}\gamma^2L_{\text{eff}}^2\sum_{j=1}^{N_c}\frac{2-\delta_{nj}}{\Delta f^2}\Psi_{nj} \quad (29)$$

(where we used the GN values in Section III) such that the approximate OPT power profile is

$$P_k = \left(\frac{P_{A1,k}}{2\alpha_{\text{NL1},k}}\right)^{1/3} \quad (30)$$

and this profile implies a 3 dB power ratio between ASE and NLI power at all channels.

We may also look for the AIR-maximizing per-channel power P in the case of a CIP (i.e., flat) TX power profile. In such a case we may define a WDM averaged NLI coefficient

$$<\alpha_{\text{NL1},k}> \triangleq \frac{1}{N_c}\sum_{k=1}^{N_c}\alpha_{\text{NL1},k} \quad (31)$$

and a WDM averaged ASE power $<P_{A1,k}>$, and use the approximation that droop (20) is channel independent, i.e.,

$$\chi(P) \cong \left(1+<\alpha_{\text{NL1},k}>P^2+\frac{<P_{A1,k}>}{P}\right)^{-1} \quad (32)$$

and look for P that maximizes $\text{SNR} = \frac{1}{(\chi^{-1})^M-1}$, thus that minimizes χ^{-1}, hence that minimizes $<\alpha_{\text{NL1},k}>P^2+\frac{<P_{A1,k}>}{P}$. By differentiating w.r.t. P we find that the (approximate) optimal

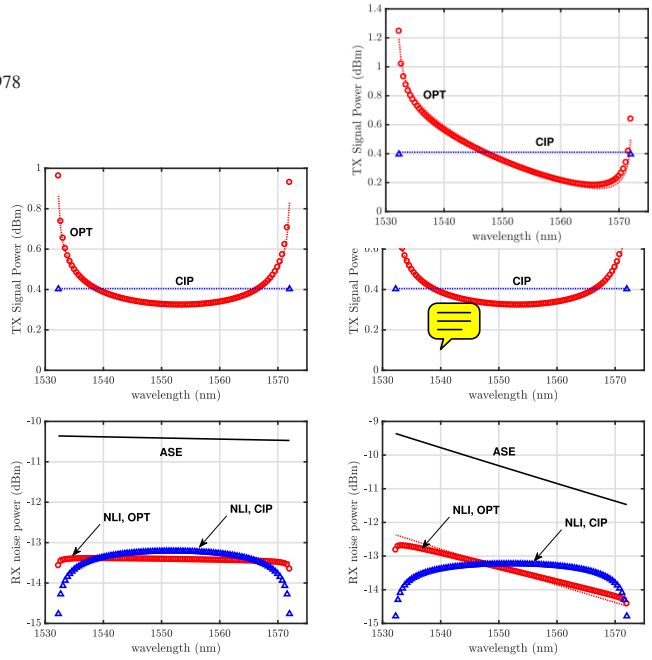

Fig. 13. TX WDM power (top row) and RX noise power (NLI, ASE, bottom row) vs. wavelength for (left column) flat noise figure, and (right column) 2 dB-tilted noise figure, both with average value 4.5 dB. Symbols: exact optimal profiles. Dotted OPT profile is (30). Dotted CIP line is (33). Link data as in [43, Figs. 2, 3]: 40×100 km SMF link, span loss $A = 21$ dB, dispersion $D = 17$ ps/nm/km, nonlinear coefficient $\gamma = 1.4\,\mathrm{W}^{-1}\,\mathrm{km}^{-1}$, gap $\Gamma = -1$ dB, channel bandwidth and spacing $\Delta f = 50$ GHz. Gaussian modulation.

CIP per-channel power is [25]:

$$P^* = \left(\frac{< P_{A1,k} >}{2 < \alpha_{\mathrm{NL1},k} >} \right)^{1/3}. \tag{33}$$

For a numerical appreciation of the above formulas and comparison with existing literature, we consider here the same 100-channel 40×100 km SMF link tackled in [43], with span loss $A = 21$ dB, dispersion $D = 17$ps/nm/km, nonlinear coefficient $\gamma = 1.4\ \mathrm{W}^{-1}\ \mathrm{km}^{-1}$, noise figure 4.5 dB, gap $\Gamma = -1$ dB, channel bandwidth and channel spacing equal to $\Delta f = 50$ GHz, with Gaussian modulation to meet the GN model assumptions. Fig. 13(top row) shows both the TX OPT power profile, and the CIP (i.e. flat) power profile that maximize AIR, both for a frequency flat noise figure (left column, Cfr. [43, Figs. 2, 3]) and for a 2-dB tilted noise figure (left column), both at the same average noise figure 4.5 dB. Symbols are the exact optima, obtained by a nonlinear solver [43]. The dotted line for OPT is (30), and that for CIP is (33), and both are seen to be very good approximations to the exact solutions.[4] We also verified that the CIP optimal power P^* is in both cases essentially coinciding with the WDM-average of the OPT power profile, i.e.:

$$P^* = \left(\frac{< P_{A1,k} >}{2 < \alpha_{\mathrm{NL1},k} >} \right)^{1/3} \simeq < \left(\frac{P_{A1,k}}{2\alpha_{\mathrm{NL1},k}} \right)^{1/3} > . \tag{34}$$

Fig. 13(bottom row) shows the corresponding received ASE and NLI power profiles after $M = 40$ spans. Again symbols are for the exact solutions. We see that for both noise figure profiles, the OPT-generated NLI is roughly 3 dB below the ASE profile (the dotted line in the bottom right figure is an exact down-shift by 3 dB of the ASE profile). In summary, the AIR-maximizing (pump-unconstrained) TX power allocation is such that the generated NLI profile is roughly 3 dB below the ASE profile, and the optimal TX power profile has a convex shape with a tilt that follows that of the noise figure profile. Formulas (33) and (30) are new, and will be used extensively in the main text.

[4]We note that the CIP optimal power for a flat noise figure reported in [43, Fig. 2] is 0.26 dBm, while with our closed-form GN formulas in Section III we get here 0.4 dBm. We verified that the exact GN model (which uses double frequency integrations [25]) is consistent with the reported 0.4 dBm.

REFERENCES

[1] T. Frishch and S. Desbruslais, "Electical power, a potential limit to cable capacity," in *Proc. SubOptic*, Paris, France, 2013, pp. TUIC-0 4.

[2] O. V. Sinkin et al., "Maximum optical power efficiency in SDM-based optical communication systems," *IEEE Photon. Technol. Lett.*, vol. 29, no. 13, pp. 1075–1077, May 2017.

[3] O. V. Sinkin et al., "SDM for power-efficient undersea transmission," *J. Lightw. Technol.*, vol. 36, pp. 361–371, Jan. 2018.

[4] R. Dar et al., "Cost-optimized submarine cables using massive spatial parallelism," *J. Lightw. Technol.*, vol. 36, no. 18, pp. 3855–3865, Sep. 2018.

[5] J. D. Downie, "Maximum capacities in submarine cables with fixed power constraints for c-band, c l band, and multicore fiber systems," *J. Lightw. Technol.*, vol. 36, no. 18, pp. 4025–4032, Sep. 2018.

[6] P. Pecci et al., "Pump farming as enabling factor to increase subsea cable capacity," in *Proc. Suboptic*, New Orleans, la, usa, 2019, pp. OP-14.4.

[7] V. Kamalov et al., "The subsea fiber as a shannon channel," in *Proc. SubOptic*, New Orleans, LA, USA, 2019, Paper OP-12.2.

[8] E. R. Hartling et al., "Subsea open cables: A practical perspective on the guidelines and gotchas," in *Proc. SubOptic*, New Orleans, LA, USA, 2019, pp. 1–56.

[9] J.-C. Antona, A. Carbo-Meseguer, and V. Letellier, "Evolution of high capacity submarine open cables," in *Proc. Asia Commun. Photon. Conf.*, Chengdu, China, 2019, Paper S4B.2.

[10] J.-C. Antona et al., "Performance of open cable: From modeling to wide scale experimental assessment," in *Proc. SubOptic*, New Orleans, LA, USA, 2019, pp. 7–2.

[11] J. K. Perin et al., "Importance of amplifier physics in maximizing the capacity of submarine links," *J. Lightw. Technol.*, vol. 37, no. 9, pp. 2076–2085, May 2019.

[12] J. D. Downie, X. Liang, and S. Makovejs, "Assessing capacity and cost/capacity of 4-Core multicore fibers against single core fibers in submarine cable systems," *J. Lightw. Technol.*, vol. 38, no. 11, pp. 3015–3022, Jun. 2020.

[13] M. A. Bolshtyansky et al., "Single-mode fiber SDM submarine systems," *J. Lightw. Technol.*, vol. 38, no. 6, pp. 1296–1304, Mar. 2020.

[14] J. D. Downie, X. Liang, and S. Makovejs, "Examining the case for multicore fibers in submarine cable systems based on fiber count limits," *IEEE J. Sel. Topics Quantum Electron.*, vol. 26, no. 4, pp. 1–9, Jul./Aug. 2020.

[15] J. D. Downie et al., "Experimental characterization of power efficiency for power-limited SDM submarine transmission systems," in *Proc. Eur. Conf. Opt. Commun.*, Brussels, Belgium, 2020, pp. 1–4.

[16] E. R. Hartling et al., "Design, acceptance and capacity of subsea open cables," *J. Lightw. Technol.* vol. 39, pp. 742–756, Feb. 2021.

[17] X. Liang, J. D. Downie, and J. E. Hurley, "Repeater power conversion efficiency in submarine optical communication systems," *IEEE Photon. J.*, vol. 13, no. 1, Feb. 2021, Art. no. 7901110.

[18] H. Srinivas et al., "Modeling and experimental measurement of power efficiency for power-limited SDM submarine transmission systems," *J. Lightw. Technol.* vol. 39, no. 8, pp. 2376–2386, Apr. 2021.

[19] J. D. Downie, X. Liang, and S. Makovejs, "Modeling the techno-economics of multicore optical fibers in subsea transmission systems," *J. Lightw. Technol.*, vol. 40, no. 6, pp. 1569–1578, Mar. 2022.

[20] C. R. Giles and E. Desurvire, "Propagation of signal and noise in concatenated erbium-doped fiber optical amplifiers," *J. Lightw. Technol.*, vol. 9, no. 2, pp. 147–154, Feb. 1991.

[21] A. Bononi et al., "A state-variable approach to submarine links capacity optimization," *J. Lightw. Technol.*, vol. 29, no. 18, pp. 5753–5765, Sep. 2021.

[22] Y. Sun, J. L. Zyskind, and A. K. Srivastava, "Average inversion level, modeling, and physics of erbium-doped fiber amplifiers," *J. Sel. Topics Quantum Electron.*, vol. 3, no. 4, pp. 991–1007, Aug. 1997.

[23] A. Bononi and L. A. Rusch, "Doped-fiber amplifier dynamics: A system perspective," *J. Lightw. Technol.*, vol. 16, no. 5, pp. 945–956, May 1998.
[24] P. Poggiolini, "The GN model of non-linear propagation in uncompensated coherent optical systems," *J. Lightw. Technol.*, vol. 30, no. 24, pp. 3857–3879, Dec. 2012.
[25] P. Poggiolini et al., "The GN-model of fiber non-linear propagation and its applications," *J. Lightw. Technol.*, vol. 32, no. 4, pp. 694–721, Feb. 2014.
[26] A. Bononi et al., "Capacity maximization of power-constrained submarine systems," in *Proc. Opt. Fiber Commun. Conf.*, San Diego, CA, USA, 2022, Paper M2C.3.
[27] J. Antona, A. C. Meseguer, and V. Letellier, "Transmission systems with constant output power amplifiers at low SNR values: A generalized droop model," in *Proc. Opt. Fiber Commun. Conf.*, San Diego, CA, USA, 2019, Paper M1J.6.
[28] A. Bononi, J.-C. Antona, A. C. Meseguer, and P. Serena, "A model for the generalized droop formula," in *Proc. Eur. Conf. Opt. Commun.*, Dublin, Ireland, 2019, Paper W.1.D.5.
[29] A. Bononi, J. C. Antona, and P. Serena, "The generalized droop model for optical long-haul transmission systems," in *Proc. Eur. Conf. Opt. Commun.*, Brussels, Belgium, 2020, pp. 1–4.
[30] J. D. Downie, X. Liang, P. Sterlingov, N. Kaliteevskiy, and V. Ivanov, "Extension of SNR droop model for constant output power amplifier systems," in *Proc. Eur. Conf. Opt. Commun.*, Dublin, Ireland, 2019, pp. 1–4.
[31] A. Bononi et al., "The generalized droop formula for low signal to noise ratio optical links," *J. Lightw. Technol.*, vol. 38, no. 8, pp. 2201–2213, Apr. 2020.
[32] J. D. Downie et al., "SNR model for generalized droop with constant output power amplifier systems and experimental measurements," *J. Lightw. Technol.*, vol. 38, no. 12, pp. 3214–3220, Jun. 2020.
[33] A. Bononi et al., "The generalized droop model for submarine fiber-optic systems," *J. Lightw. Technol.*, vol. 39, no. 16, pp. 5248–5257, Aug. 2021.
[34] P. Poggiolini et al., "A detailed analytical derivation of the GN model of non-linear interference in coherent optical transmission systems," Sep. 2012, *arXiv:1209.0394v13*.
[35] P. Serena, "Nonlinear signal–noise interaction in optical links with nonlinear equalization," *J. Lightw. Technol.*, vol. 34, no. 6, pp. 1476–1483, Mar. 2016.
[36] A. Ghazisaeidi, "A theory of nonlinear interactions between signal and amplified spontaneous emission noise in coherent wavelength division multiplexed systems," *J. Lightw. Technol.*, vol. 35, pp. 5150–5175, Dec. 2017.
[37] T. Georges and E. Delevaque, "Analytic modeling of high-gain erbium-doped fiber amplifiers," *Opt. Lett*. vol. 17, no. 16, pp. 1113–111, Aug. 1992.
[38] A. A. M. Saleh et al., "Modeling of gain in erbium-doped fiber amplifiers," *IEEE Photon. Technol. Lett*. vol. 2, no. 10, pp. 714–717, Oct. 1990.
[39] F. Forghieri, R. W. Tkach, A. R. Chraplyvy, and J. Nagel, "Effect of amplifier gain shape on optical nonlinearity penalties," in *Proc. Opt. Amplifiers Their Appl.* Davos, Switzerland, 1995, Paper SaB2-1.
[40] W. Yu and J. M. Cioffi, "On constant power water-filling," in *Proc. IEEE Int. Conf. Commun.*, Helsinki, Finland, 2001, vol. 6, pp. 1665–1669.
[41] A. Bononi, P. Serena, and J.-C. Antona, "Gain-shaped waterfilling is quasi-optimal for constant-pump Flattened-EDFA submarine links," in *Proc. Eur. Conf. Opt. Commun.*, Brussels, Belgium, 2020, pp. 1–4.
[42] A. Bononi, N. Rossi, and P. Serena, "On the nonlinear threshold versus distance in long-haul highly-dispersive coherent systems," *OSA Opt. Exp.*, vol. 20, no. 26, pp. B204–B216, Dec. 2012.
[43] I. Roberts, J. M. Kahn, and D. Boertjes, "Convex channel power optimization in nonlinear WDM systems using Gaussian noise model," *J. Lightw. Technol.*, vol. 34, no. 13, pp. 3212–3222, Jul. 2016.
[44] E. Desurvire, J. W. Sulhoff, J. L. Zyskind, and J. R. Simpson, "Study of spectral dependence of gain saturation and effect of inhomogeneous broadening in erbium-doped aluminosilicate fiber amplifiers," *IEEE Photon. Technol. Lett.*, vol. 2, no. 9, pp. 653–655, Sep. 1990.
[45] M. Bolshtyansky, "Spectral hole burning in erbium-doped fiber amplifiers," *J. Lightw. Technol.*, vol. 21, no. 4, pp. 1032–1038, Apr. 2003.
[46] A. Pilipetskii et al., "Spectral hole burning simulation and experimental verification in long-haul WDM systems," in *Proc. Opt. Fiber Commun. Conf.*, Atlanta, GA, USA, 2003, Paper ThW2.
[47] A. Pilipetskii et al., "Spectral hole-burning in long-haul WDM transmission," in *Proc. Opt. Fiber Commun. Conf.*, Los Angeles, CA, USA, 2004, Paper FM3.